Video Article

Methods for Measuring the Orientation and Rotation Rate of 3D-printed Particles in Turbulence

Brendan C. Cole[1], Guy G. Marcus[1], Shima Parsa[1], Stefan Kramel[1], Rui Ni[1], Greg A. Voth[1]

[1]Department of Physics, Wesleyan University

Correspondence to: Greg A. Voth at gvoth@wesleyan.edu

URL: https://www.jove.com/video/53599
DOI: doi:10.3791/53599

Keywords: Engineering, Issue 112, particles in turbulence, anisotropic particles, turbulence, 3D printing, rotation, fluid dynamics

Date Published: 6/24/2016

Citation: Cole, B.C., Marcus, G.G., Parsa, S., Kramel, S., Ni, R., Voth, G.A. Methods for Measuring the Orientation and Rotation Rate of 3D-printed Particles in Turbulence. *J. Vis. Exp.* (112), e53599, doi:10.3791/53599 (2016).

Abstract

Experimental methods are presented for measuring the rotational and translational motion of anisotropic particles in turbulent fluid flows. 3D printing technology is used to fabricate particles with slender arms connected at a common center. Shapes explored are crosses (two perpendicular rods), jacks (three perpendicular rods), triads (three rods in triangular planar symmetry), and tetrads (four arms in tetrahedral symmetry). Methods for producing on the order of 10,000 fluorescently dyed particles are described. Time-resolved measurements of their orientation and solid-body rotation rate are obtained from four synchronized videos of their motion in a turbulent flow between oscillating grids with $R_\lambda = 91$. In this relatively low-Reynolds number flow, the advected particles are small enough that they approximate ellipsoidal tracer particles. We present results of time-resolved 3D trajectories of position and orientation of the particles as well as measurements of their rotation rates.

Video Link

The video component of this article can be found at https://www.jove.com/video/53599/

Introduction

In a recent publication, we introduced the use of particles made from multiple slender arms for measuring rotational motion of particles in turbulence[1]. These particles can be fabricated using 3D printers, and it is possible to accurately measure their position, orientation, and rotation rate using multiple cameras. Using tools from slender body theory, it can be shown that these particles have corresponding effective ellipsoids[2], and the rotational motions of these particles are identical to those of their respective effective ellipsoids. Particles with symmetric arms of equal length rotate like spheres. One such particle is a jack, which has three mutually perpendicular arms attached at its center. Adjusting the relative lengths of the arms of a jack can form a particle equivalent to any tri-axial ellipsoid. If the length of one arm is set equal to zero, this creates a cross, whose equivalent ellipsoid is a disk. Particles made of slender arms take up a small fraction of the solid volume of their solid ellipsoidal counterparts. As a result, they sediment more slowly, making them easier to density match. This allows the study of much larger particles than is convenient with solid ellipsoidal particles. Additionally, imaging can be performed at much higher particle concentrations because the particles block a smaller fraction of the light from other particles.

In this paper, methods for fabrication and tracking of 3D-printed particles are documented. Tools for tracking the translational motion of spherical particles from particle positions as seen by multiple cameras have been developed by several groups[3,4]. Parsa *et al.*[5] extended this approach to track rods using the position and orientation of the rods seen by multiple cameras. Here, we present methods for fabricating particles of a wide variety of shapes and reconstructing their 3D orientations. This offers the possibility to extend 3D tracking of particles with complex shapes to a wide range of new applications.

This technique has great potential for further development because of the wide range of particle shapes that can be designed. Many of these shapes have direct applications in environmental flows, where plankton, seeds, and ice crystals come in a vast array of shapes. Connections between particle rotations and fundamental small-scale properties of turbulent flows[6] suggest that study of rotations of these particles provides new ways to look at the turbulent cascade process.

Protocol

1. Fabrication of Particles

1. Use a 3D Computer Aided Drafting program to create particle models. Export one file per model in a file format that can be processed by the 3D printer used.
    1. Use the Circle command to draw a circle with a diameter of 0.3 mm. Use the Extrude function to make a cylinder with a length of 3 mm.

2. Make a cross with two orthogonal cylinders with a common center; make a jack with three mutually orthogonal cylinders with a common center; make a tetrad with four cylinders sharing a common end at 109.5° angles to one another; make a triad with three cylinders in a plane sharing a common end at 120° angles to one another.
3. To tilt cylinders (hereafter called "arms" of the particles) with respect to one another, use the Rotate 3D command to draw a line across the diameter of the circle at one of its ends and then enter the desired angle of rotation.
4. Use the Union command to join the different arms together into a single watertight object.
5. Use Rotate 3D again to tilt the object so that no arms are along the vertical or horizontal axes, because arms that lie along these axes tend to have defects, break off more easily, or flatten out.
6. Export each object in a separate file in a format that can be used by 3D printers.

2. Order approximately 10,000 particles of each type from a commercial source that specializes in additive manufacturing or print them at an available facility. Particles should be printed on a polymer extrusion printer that uses a support matrix of a different material that can be dissolved away.
    1. Order the particles three weeks or more before experiments are planned because the arrangement and printing of so many particles is a slow process. Ensure that particles are printed on "high-resolution mode" because the particles are near the minimum feature size of many 3D printers and the arms will not be as symmetric and may break if printed at lower resolution.

2. Preparation of Particles

1. Prepare a salt solution in which the particles are neutrally buoyant to minimize particles' arms bending while in storage and so that gravitational and buoyancy forces do not have to be accounted for in the analysis.
    1. Test average particle densities by immersing particles in solutions of water mixed with calcium chloride ($CaCl_2$) at densities around 1.20 g/cm^3.
        1. To determine water density, first zero a scale while an empty 100 ml volumetric flask is on top of it. Take the flask off and fill it with water mixed with $CaCl_2$. Place the flask back atop the scale and divide the given mass by 100 ml.
        Note: Because 1 ml = 1 cm^3, 1 g/ml = 1 g/cm^3.
        2. Test particles at many different solution densities, ranging from 1.16 g/cm^3 to 1.25 g/cm^3, in roughly 0.01 g/cm^3 increments. Test multiple particles at every density because not all particles will have the same density: in the same solution, some will sink, some will be neutrally buoyant, and some will float.

    2. Record at which density particles are, on average, neutrally buoyant after several hours.
    Note: The density found may be significantly different from the bulk density quoted by the particle manufacturers.
    3. Mix about 400 kg of $CaCl_2$ into approximately 1,600 L of water until the solution is at the density recorded in 2.1.1 - 2.1.2.
    4. Remove about 1 L of this mixed solution per particle type (jacks, tetrads, *etc.*) to be used for storage of particles. Hold each liter in a different container at room temperature. Store the remainder of the solution at room temperature in a large storage tank.

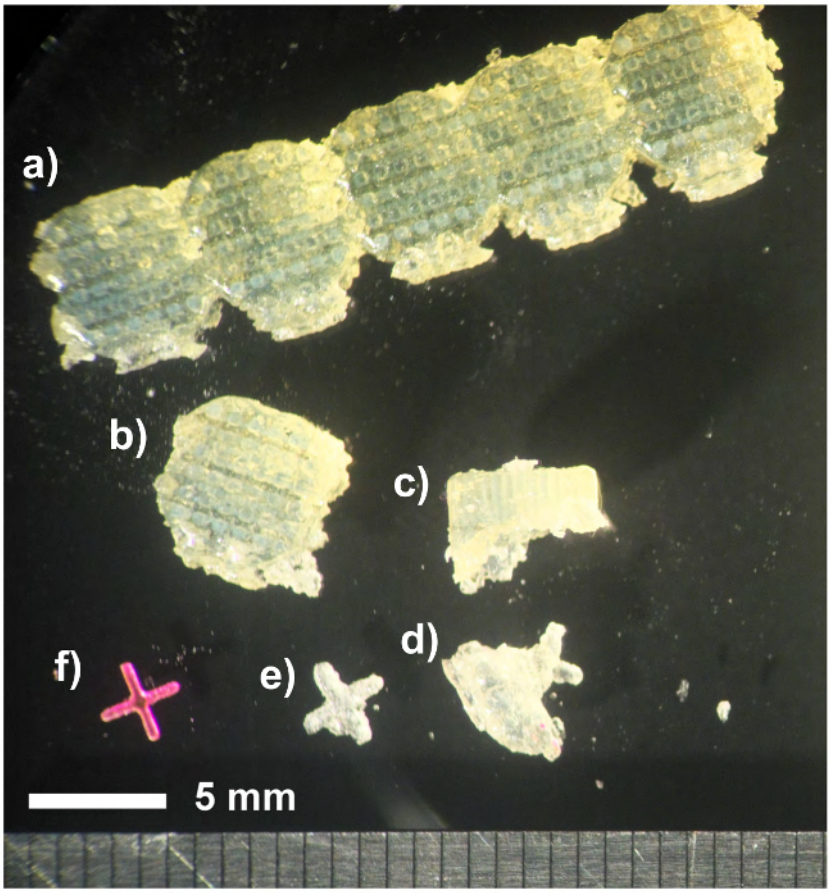

Figure 1. A jack at various stages of resin removal. a) The blocks of support resin that the particles arrive in. **b**) A single block separated from the rest. **c-e**) Multiple stages of resin removal done by hand. **f**) A single jack after the NaOH bath and Rhodamine-B dye. Please click here to view a larger version of this figure.

2. Manually loosen the support material in which the particles come encased by gently breaking the large pieces (~ 5 mm x 320 mm, part of which is shown in **Figure 1a**) into small sections (~5 mm x 5 mm, **Figure 1b**), then manually massage each section until much of the excess resin has come off (**Figure 1c-e**). Remove excess resin in this way to reduce the amount of the NaOH solution that will need to be created for steps 2.2.1 - 2.2.4.
    1. Place the remaining resin block in a 10% by mass sodium hydroxide (NaOH) solution immersed in an ultrasonic bath for one hour. The resin is a different material than the particles are, so the NaOH will remove the resin without permanently affecting the particles.
    CAREFUL: The solution is corrosive and will get hot while in the ultrasonic bath.
    2. Filter out particles.
        1. To filter particles, create a funnel using netting with 0.1016 cm x 0.13462 cm plastic holes. Hold the funnel over the container to be used for the disposal of the NaOH solution and slowly pour the solution through. Dispose of NaOH solution in accordance with environmental health and safety guidelines.
    3. Rinse particles gently with water before immersing in a new 10% by mass NaOH solution in an ultrasonic bath for another half hour.
    4. Filter out particles as in 2.2.2.1 and store in the density-matched solution separated in 2.1.4 while they harden. Handle the particles carefully because the NaOH solution temporarily softens them.
    Note: If particles are not stored in a density-matched solution, some arms may bend. Keeping them immersed in the density-matched solution for several hours also allows some voids in the plastic to fill with fluid.

3. Dye particles with Rhodamine-B mixed with water so that they fluoresce under the light emitted by a green laser.
    1. Prepare a 1 L solution of Rhodamine-B dye in water at a concentration of 0.5 g/L (afterward referred to as "dye").
    CAUTION: Toxic.
    2. Heat the dye to a temperature between 50 and 80 °C, depending on particle material. Use higher temperatures for harder plastics; using too high of a temperature will result in the arms bending.
    3. Put ~2,500 particles, enough to loosely fill ~25 ml in the density-matched storage solution, in the dye and keep all at 80 °C for two to three hours to allow the dye to absorb into the polymer. Remove particles once they are pink, like the one in **Figure 1f**.
    CAREFUL: The heat will soften the particles temporarily.
    4. Filter out particles and rinse them before storage in the designated solutions separated in 2.1.4. The particles will lose a small fraction of their dye, making the solution pink, but rinsing under the faucet helps prevent losing a detrimental amount of dye.
    Note: Average particle density will have changed due to dyeing, so test again as in 2.1.1-2.1.2 to find the new solution density at which particles are, on average, neutrally buoyant.

4. Change bulk $CaCl_2$ solution (from 2.1.3) density as needed. Repeat 2.1.4 and remove new volumes of density-matched solution. Dispose of former storage solutions, which will now have small amounts of Rhodamine-B dye in them, in accordance with environmental health and safety regulations.
5. Repeat 2.3.2-2.3.4 for successive sets of ~2,500 particles, storing all particles of the same shape in the same density-matched solutions created in 2.4, separated from particles of different shapes.
   Note: After about 5 repetitions of 2.3.2-2.3.4, the Rhodamine-B solution will no longer be a high enough concentration to effectively dye particles.
6. Dispose of the solution created in 2.3.1 in accordance with environmental health and safety regulations, then repeat 2.3.1 and create a new 0.5 g/L solution with which to dye particles.
7. Repeat 2.6 every 5 repetitions of 2.3.2-2.3.4.

3. Experimental and Optical Setup

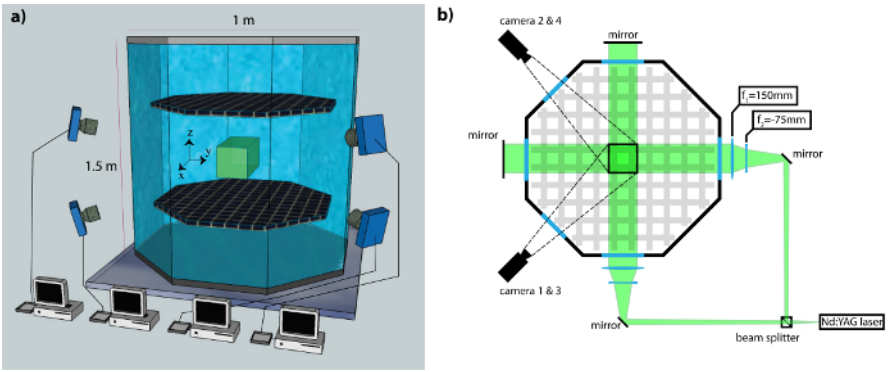

Figure 2. Experimental setup. In the octagonal flow between oscillating grids, a central viewing volume in the focus of the four video cameras is illuminated by a green Nd:YAG laser. **a**) Side view showing how the four cameras are arranged and connected to computers. Figure from [13]. **b**) Top view showing laser, mirror, and lens configuration to achieve uniform illumination in the central volume. Please click here to view a larger version of this figure.

1. Prepare the cameras.
   1. Use cameras capable of at least 1 megapixel resolution at 450 frames per second.
   2. Arrange the cameras such that each camera is pointing at, and is focused on, the center of the viewing volume. Fewer cameras can be used, however shadowing of an arm of a particle by another arm limits the orientation measurement accuracy, and having fewer cameras makes experiments more susceptible to this effect. Using more than four cameras could likewise increase orientation measurement precision because it will reduce the chance of arms being shadowed on all cameras, which is a primary source of uncertainty.
   3. Position the cameras with large (~90°) angles between each pair subject to constraints of the apparatus. Place cameras as shown in **Figure 2** to balance experimental access and the size of the angle between individual cameras. Minimize optical distortions by building viewing ports into the apparatus perpendicular to each camera viewing direction.
   4. Use 200 mm macro lenses on each camera to obtain the desired measurement volume from a working distance of half a meter. The volume viewed by all four cameras determines the detection volume, which is about 3 x 3 x 3 cm^3.
   5. Calibrate the cameras to allow transformation from measured pixel positions to coordinates in 3D space.
      1. Set the apertures to f/11 and mount 532 nm notch filters to remove laser light while allowing through longer-wavelength fluorescence onto the cameras
      2. Place an image calibration mask in the tank, fill the tank with the bulk solution from 2.4, and illuminate the mask.
      3. Adjust the cameras so they each have the mask in view and they all are focused on the same point on the mask. Carefully align the cameras to optimize the shape of the detection volume.
      4. Be careful to change as little as possible about the optical setup from this point forward.
      5. Acquire and store images of the mask from each camera.
      6. Drain the solution out of the tank and pump it back where it had previously been stored.
      7. Extract the parameters specifying the position, viewing direction, magnification, and optical distortions of each camera from the calibration images. Do this by identifying places on the calibration mask visible on all four cameras and defining the distance between these points. With this information, use standard calibration methods to extract relevant parameters.
         Note: The basic calibration method is described in Tsai, 1987[7]. The implementation used in these experiments is described in Oullette *et al.*[3] Researchers wishing to develop camera calibration software may also want to consider OpenPTV[4].
      8. Create a final calibration file using a dynamic calibration process. This is done after tracer particle data has been acquired. Use a nonlinear least squares search to optimize the camera calibration parameters and obtain the smallest mismatch between the positions of particles seen on multiple cameras. These methods are described in Ref. [8] and [9].

2. With a Q-switched green Nd:YAG laser capable of 50 W average power (hereafter called the "laser"), illuminate a cylinder in the center of the tank with roughly a 3 cm cross-sectional diameter, where the flow is homogeneous.[8]
   Note: The laser power is specified at a pulse frequency of 5 kHz. The pulse frequency in these experiments is 900 Hz, where the output power is significantly lower.
   1. Split the light from the laser using a beam splitter and use mirrors to guide one beam into the front of the tank and the other, orthogonal to the first, into the side of the tank.

2. Place two additional mirrors outside of the tank, opposite where the beams are entering, in order to reflect light back into the tank and create more uniform illumination, dramatically decreasing shadowing effects.
   Note: The length scale of interference effects from the counter-propagating beams is too small to significantly affect these experiments.

4. Perform the Experiments

1. Prepare to record video from each camera.
   1. Program an image compression system that removes unwanted image data in real time.[10,13]
      1. If the camera does not have a particle in view, do not save the image.
      2. Where there are bright pixels, save only the location and brightness of bright pixels instead of the whole image.
         Note: Because each particle typically covers approximately 5,000 bright pixels and there is rarely more than one particle in view at a time, the image compression system dramatically reduces the amount of storage required to record with high-speed cameras for many hours.
   2. Prepare the data acquisitioning software.
2. Prepare the turbulent flow in a 1 x 1 x 1 m^3 octagonal tank using two parallel 8 cm mesh grids oscillating in phase.[8]
   1. Pump the $CaCl_2$ solution from 2.4 into a vacuum chamber and keep it in the chamber overnight to degas the solution, which minimizes air bubbles in the experiments.
   2. Pump solution from the vacuum chamber through a 0.2 µm filter into the octagonal tank where experiments will be performed.
3. Run the experiment.
4. Choose one particle type (tracer particles, jacks, crosses, tetrads, or triads) to be used for the first round of experiments and add all 10,000 of those particles into the water through a port at the top of the apparatus. Close this port after adding particles.
   1. Turn the laser on.
   2. Set cameras and laser to respond to an external trigger and set the frequency of the trigger to 450 Hz for the cameras and 900 Hz for the laser. Use the external trigger to ensure all cameras start acquisition simultaneously and remain synchronized throughout the recording
   3. Open the laser aperture.
   4. Set the grid to the chosen frequency (1 or 3 Hz) and start it running. Before starting data acquisition, run the grid for about 1 min to allow turbulence to fully develop.
   5. Record 10^6 frames in order to keep the file size manageable and to keep any errors that may occur in the image compression systems from compromising too much data.
   6. Close the laser aperture and stop the camera trigger. Reset the image compression systems and the cameras.
      1. Check that the video files are not corrupted by viewing portions of each file.
   7. Repeat 4.4.1 - 4.4.6 until 10^7 images have been recorded at the chosen grid frequency for the chosen particle.
5. Change the grid frequency to the one not chosen in 4.4.4 and repeat 4.4.4 - 4.4.7
6. Empty the tank and filter the water to remove all particles. Save particles in the storage water from 2.4 if desired.
7. Repeat 4.4 - 4.6 for all particle types.
8. After all experiments have been finished, calibrate cameras once more, as in 3.1.5-3.1.5.7.

5. Data Analysis

Note: This section of the Protocol presents an overview of the process used to obtain particle orientations and rotation rates. The specific programs used, along with test images and calibration files, are included as a supplement to this publication, and are open to use by any interested readers. (See the file "Use_Instructions.txt" in the supplemental file "MATLAB_files.zip".)

1. Using the camera calibration parameters, obtain the 3D position and orientation from images of particles on multiple cameras.
   1. At every frame, find the center of the particle on each of the four images. All particles in these experiments are sufficiently symmetric that the center of the object is at the geometric center of the bright pixels on the image when viewed from any perspective.
   2. Find the 3D position of the particle by stereomatching its simultaneous 2D positions on all four cameras[3,8].
   3. Create a numerical model of the particle that can be projected onto each camera to model the intensity in the image from that camera.
      1. Model the particle as a composite of rods. Using the camera calibration parameters from 3.1.5.7 and 3.1.5.8, project the two end points of each rod onto the cameras and then model the distribution of light intensity in two dimensions, with a Gaussian function across the width of the rod and a Fermi-Dirac function across its length according to software protocol.
      2. Model light intensity in two dimensions in this way to minimize the computational cost of the data analysis. Projection of a full three-dimensional model of the fluorescent particle could improve on this approach, but would be much more computationally intensive.
      3. Click Run to begin analysis.
   4. Choose an initial guess of the particle orientation.
      1. If analyzing the first frame in which this particle is visible, the first guess can be a random set of Euler angles.
      2. If this particle was in at least one previous frame, use the orientation found using the previous frame as the initial guess.
   5. Perform a nonlinear least-squares fit to determine the particle orientation.
      1. Optimize the three 3D position coordinates and the three Euler angles such that the squared difference between the measured intensity and the 2D projection of the model is minimized on all four cameras according to software protocol.

Note: There are multiple conventions for defining Euler angles. Define the angles, (φ, θ, ψ) , as follows: φ is an initial rotation about the z axis, creating new axes *x′* and *y′*; θ is a rotation about *x′*, creating new axes *z′* and *y″*; ψ is a rotation about the new *z′* axis.[11]

6. Choose the orientation that requires the smallest rotation with respect to the previous frame. For a jack, the Euler angles found give one of the 24 symmetric orientations; for a tetrad it is one of 12 symmetric orientations; for a cross, it is one of 8 symmetric orientations; and for a triad it is one of 6 symmetric orientations.
Note: The method in 5.1.6 assumes that the particle will not rotate more than half of one of its interior angles between frames. Justification for this assumption is given in the Discussion.

2. Save the position and Euler angles as a function of time.
3. Use these data to extract solid-body rotation rate and other quantities.

Representative Results

Figure 3a shows an image of a tetrad from one of our cameras above a plot of the Euler angles obtained from a section of its trajectory (**Figure 3c**). In **Figure 3b**, the results of the orientation-finding algorithm, described in Protocol 5 - 5.3, are superimposed on the tetrad image. The arms of the tetrad in **Figure 3a** do not follow the simple intensity distributions that are used to create the model (Protocol 5.1.3.1). This is true for all of the particles. The observed intensity furthermore has a non-trivial dependence on the angles between the arms, the illumination, and the viewing direction[12]. The models do not include any of these factors but nonetheless produce very accurate measurements of particle orientations.

Once an orientation is found with a least-squares fit, the 3D coordinates of the particle center and the three Euler angles, (φ, θ, ψ) , that specify its orientation matrix[11] are saved. This is done for every frame where the particle is in view of all four cameras. These data enable the reconstruction of the complete trajectory of the particle across the viewing volume, as are shown in **Figure 4** for a cross and a jack. **Figure 4** was made using the Paraview open source visualization package and is based on measurements made with images from the experiments.

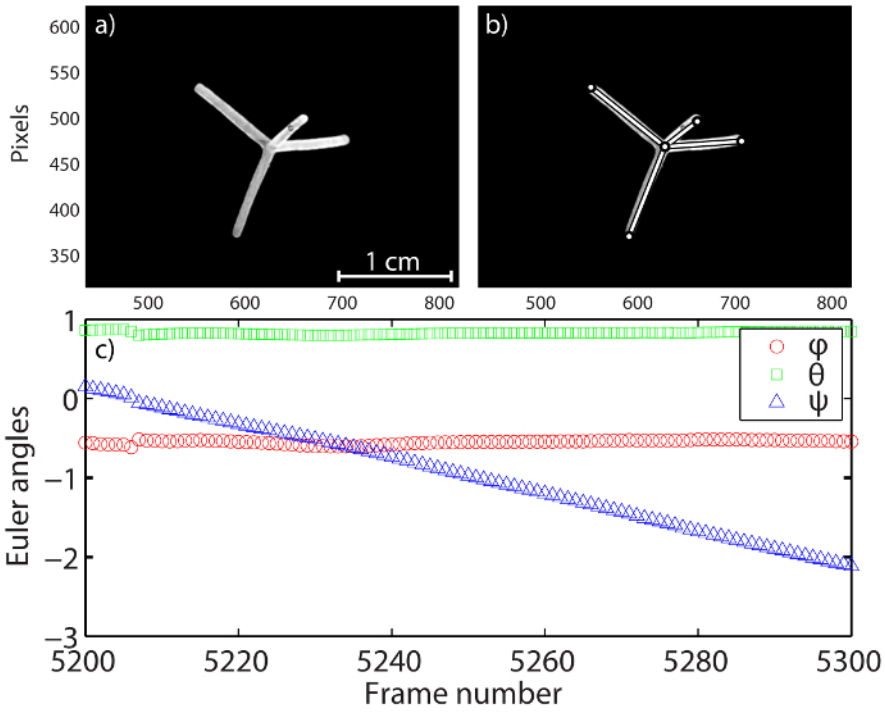

Figure 3. Reconstructed particle orientations from measured images. a) A sample image from one of the four cameras. The object shown is a tetrad, which has four arms at 109.5° interior angles to one another. **b**) The same tetrad shown with the results of our orientation-finding algorithm. **c**) Measured Euler angles plotted as a function of time for a single trajectory. Please click here to view a larger version of this figure.

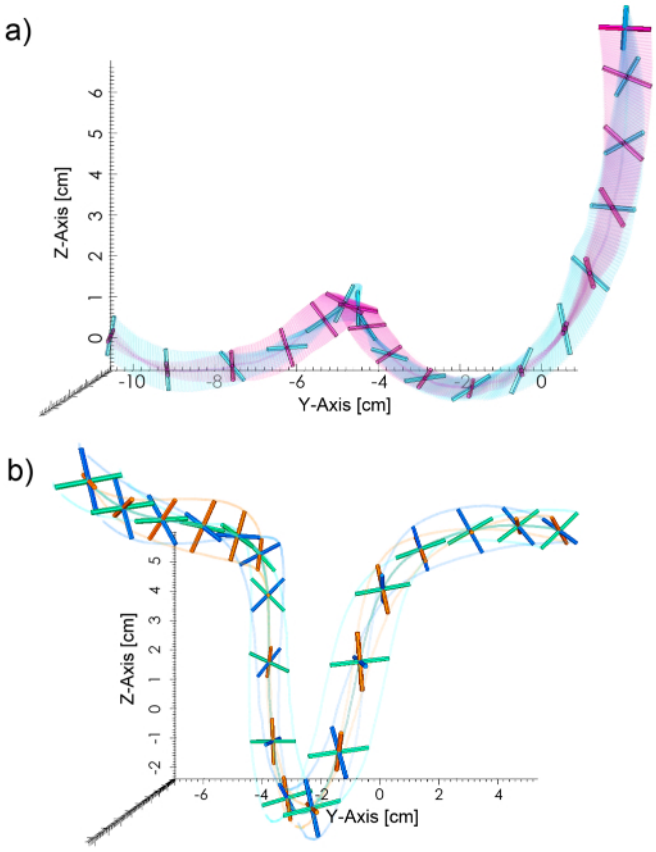

Figure 4. Reconstructed trajectories of a cross (a) and a jack (b) in three-dimensional turbulence. (**a**) The two different color sheets trace the path of the two arms of the particle through space over time. The length of the track is 336 frames, or 5.7 τ_η, and a cross is shown every 15 frames. (**b**) The blue, orange, and blue-green paths trace the paths of the three arms of the jack as the particle rotates and moves through the fluid. The dark green line denotes the path of the jack's center. The length of the particle track is 1,025 frames, or 17.5 τ_η, and a jack is shown every 50 frames. (*Note*: Neither the crosses nor the jacks above are drawn to scale.) Figure from [1], where it is Figure 3. Please click here to view a larger version of this figure.

Two different but related quantities based on particle orientations are calculated over the entire trajectory: tumbling rate and solid-body rotation rate. Tumbling rate, $\dot{\boldsymbol{p}}$, is the rate of change of the unit vector defining the orientation of the particle. In previous measurements of rods, $\boldsymbol{p}$ was defined as the axis of symmetry along the rod; for crosses and triads, $\boldsymbol{p}$ is normal to the plane of the arms; for jacks and tetrads, $\boldsymbol{p}$ is along one of the arms. Because rotation along the axis of rods cannot be directly measured, studies of the rotations of rods in turbulence have largely been limited to measuring the tumbling rate. This is not an issue for any of the particles in these experiments. All rotations of these particles can be measured and, with orientation measurements smoothed along a particle's trajectory, the full solid-body rotation rate vector, $\boldsymbol{\omega_s}$, can be found.

To extract the solid-body rotation rate from measured particles orientations, smoothing needs to be done over several time steps. The problem is to find the rotation matrix $\mathbb{R}$ that relates an initial orientation $\mathbb{O}(t_i)$ to the measured orientations $\mathbb{O}(t)$ at a sequence of time steps:

$$\mathbb{O}(t) = \mathbb{R}^{\frac{t-t_i}{\tau_f}}\,\mathbb{O}(t_i),$$

where τ_f is the period between images and t_i is the time of the initial frame. In Marcus *et al.*[1], we used a nonlinear least-squares fit to determine the six Euler angles defining the initial orientation matrix, $\mathbb{O}(t_i)$, and the rotation matrix over a single time step, $\mathbb{R}$, that best match the measured orientation matrices as a function of time. More recent work has shown that this algorithm sometimes has difficulty when the rotation rate is small because the nonlinear search is exploring the region where the Euler angles are approximately equal to zero and are degenerate. In the case where the rotation in a time step is sufficiently small, $\mathbb{R}$ can be linearized using $\mathbb{R}^{(t-t_i)/\tau_f} = \boldsymbol{\Omega}(t-t_i)$, where $\boldsymbol{\Omega}$ is a rotation rate matrix. As described in the Discussion below, these experiments are in this low rotation limit, so $\boldsymbol{\Omega}$ can be found from the measured $\mathbb{O}(t)$ using a linear least squares fit.

From the measured rotation matrix over a time step, $\mathbb{R}$, we can extract the solid-body rotation rate and the tumbling rate. By Euler's theorem[11] $\mathbb{R}$ can be decomposed as a rotation by an angle **Φ** about the solid-body rotation axis, $\hat{\boldsymbol{\omega}}_s$. The magnitude of the solid-body rotation rate is $\omega_s = {}^{\Phi}/_{\tau_f}$. The tumbling rate is the component of the solid-body rotation rate perpendicular to the orientation of the particle, and so it can be calculated as $\dot{\boldsymbol{p}} = \boldsymbol{\omega}_s \times \boldsymbol{p}$. **Figure 5** compares PDFs of the measured mean square tumbling rate for crosses and jacks to direct numerical simulations of spheres. Small jacks rotate just like spheres in fluid flows[1], so the fact that the PDF for jacks agrees with the simulated PDF for spheres demonstrates that the experiments are able to capture the rare high rotation events that occur in turbulent flows.

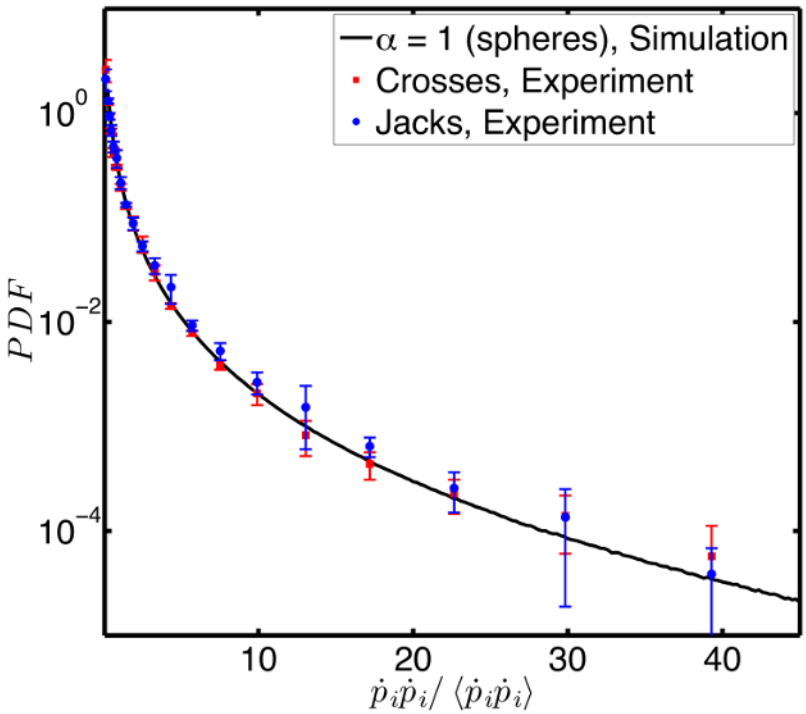

Figure 5. PDF of mean-square tumbling rate. The probability density function of the measured mean-square tumbling rate for our crosses (red squares) and jacks (blue circles) as well as direct numerical simulations of spheres (solid line). Error bars include the random error due to limited statistical sampling estimated by dividing the data set into subsets, as well as the systematic error that results from the fit length dependence of the tumbling rate, which is estimated by performing the analysis at a range of fit lengths. Figure from [1] where it is Figure 5. Please click here to view a larger version of this figure.

Discussion

Measurements of the vorticity and rotation of particles in turbulent fluid flow have long been recognized as important goals in experimental fluid mechanics. The solid-body rotation of small spheres in turbulence is equal to half the fluid vorticity, but the rotational symmetry of spheres has made direct measurement of their solid-body rotation difficult. Traditionally, the fluid vorticity has been measured using complex, multi-sensor, hot-wire probes[14]. But these sensors only get single-point vorticity measurements in airflows that have large mean velocity. Other vorticity measurement methods have been developed. For example, Su and Dahm used flow field velocimetry based on scalar images[15] and Lüthi, Tsinober, and Kinzelbach used 3D particle tracking velocimetry[16]. Measurements of vorticity in turbulence by tracking rotations of single particles were pioneered by Frish and Webb, who measured the rotations of solid spherical particles using a vorticity optical probe[17]. This probe uses small particles with planar crystals embedded that act as mirrors to create a beam whose direction changes as the particle rotates. Recently, methods have been developed for measuring the rotational motion of large spherical particles using imaging of patterns painted on the particles[18,19] or fluorescent particles embedded in transparent hydrogel particles[20]. To track anisotropic particles, Bellani *et al.* have used custom-molded hydrogel particles[21]. Parsa *et al.* have tracked the rotations of segments of nylon threads[5,6,12]. The methods for measuring vorticity and particle rotations presented in this paper have advantages over these alternative methods. 3D-printed anisotropic particles can be small, with arm thicknesses down to 0.3 mm in diameter, and their rotations can still be resolved very accurately. Other methods traditionally require larger particles because they involve the resolution of structures on or within the particles themselves. In addition, the use of image compression systems allows for many more particle trajectories to be recorded and measured than would otherwise be reasonable. Having more measurements makes it possible to study rare events like those with very high rotation rates in **Figure 5**, which reveal intermittency phenomena of great interest to researchers.

Particle concentrations in these experiments were about 5 x 10^{-3} cm^{-3}, which meant that typically only about 20% of images from the cameras had a particle. To study rare events, thousands of particle trajectories are typically required, which meant that hundreds of thousands of images of particles were needed. With these low concentrations, therefore, millions of images needed to be recorded to obtain an adequate volume of data. If real-time image compression systems were not used to facilitate data acquisition, this would require hundreds of TB of data storage and

the analysis would be much more computationally intensive. Image compression systems decrease this load by factors of several hundred[10]. However, standard video recording would be adequate for higher particle densities and if data storage space is not an issue. If 100,000 particles of each type were ordered instead of 10,000, fewer images would, in principle, be needed to capture the same statistics. However, at higher particle densities particles begin to shadow one another more often. That is, there will be more times when there are particles between the laser and the particle in view, or between the particle in view and the camera. These shadowing events make measuring orientations throughout a track across the viewing volume more difficult and less reliable. For these reasons, lower particle concentrations were chosen for these experiments and image compression systems were therefore necessary.

There may be times when arm shadowing will affect the results of the nonlinear search algorithm. For certain orientations of the jack, arm shadowing causes there to be multiple minima in Euler angle space, which lead to indeterminacies in the measured orientations. This reduces the accuracy of orientation measurements for these particular orientations and occasionally leads to erroneously high measurements of the solid-body rotation rate, which pushes additional probability density towards the tail of the PDF in **Figure 5**. For jacks, whose arms are perpendicular to each other, this issue could be decreased by changing the angles of the cameras with respect to one another to be farther away from 90°. If the configuration of the apparatus makes this change difficult to implement, one alternative is to change the geometry of the particles to decrease shadowing. This was the reason tetrads were chosen for experiments after those with jacks had been completed, and recent tetrad measurements have shown significantly improved orientation accuracy when compared to jacks.

The methods of 3D particle tracking presented here are not confined to this particular flow or the particle sizes and shapes we use. We have already begun experiments tracking tetrads and triads with much larger sizes using similar techniques. The use of high-speed cameras to measure particle orientations and rotations can be extended to a wide array of shapes and can be used for inertial particles as well as in the neutrally buoyant case presented here. Using more cameras would allow for an even wider array of potential particle shapes, as the primary limitations to this method are the resolution of the cameras and particles' self-shadowing, as discussed in the previous paragraph.

In step 5.1.6 of the Protocol, we smooth Euler angles measurements by assuming that a particle would not rotate by more than half of an angle between arms over the course of two frames — that is, we assume that the accurate orientation measurement at frame *i+1* retains the chosen symmetric orientation found for frame *i*. If the particle had rotated by more than half of one of these interior angles, then smoothing in this way would result in a sudden and incorrect reversal of the direction of rotation. In Ref. [5] we show that an upper limit on particle tumbling rate is:

$$\frac{\langle \dot{p}_i \dot{p}_i \rangle}{\langle \varepsilon \rangle / \nu} = \frac{1}{6} + \frac{1}{10}\left(\frac{\alpha^2 - 1}{\alpha^2 + 1}\right)^2.$$

So the largest tumbling rate ($\alpha = 0$ or ∞) is $\langle \dot{p}_i \dot{p}_i \rangle = \frac{4}{15\tau_\eta^2}$ which for $\tau_\eta = (\langle \varepsilon \rangle / \nu)^{1/2} = .128$ sec is 16.2 sec^{-2}. This is a root mean square (RMS) tumbling rate of 4.0 sec^{-1}. Since we record images at 450 frames per second, particles would then typically rotate 0.009 radians between frames. The smallest interior angle of any of the particles in these experiments was $\frac{\pi}{2}$, so this smoothing method would fail if particles tumble more than $\frac{\pi}{4} \approx .785$ radians between frames. Thus, we can accurately track particles with tumbling rates of more than 80 times the RMS, which is much faster than the $\sqrt{40} = 6.3$ times the RMS that we actually observe in **Figure 5**.

Disclosures

The authors have no competing financial interests to disclose.

Acknowledgements

We thank Susantha Wijesinghe who designed and constructed the image compression system we use. We acknowledge support from the NSF grant DMR-1208990.

References

1. Marcus, G., Parsa S., Kramel, S., Ni, R., and Voth, G. Measurements of the Solid-body Rotation of Anisotropic Particles in 3D Turbulence. *New J. Phys.* **16**, 102001 (2014).
2. Bretherton, F. The motion of rigid particles in a shear flow at low Reynolds number. *J. Fluid Mech.* **14** (02), 284-304 (1962).
3. Oullette, N., Xu, H., Bodenschatz, E. A quantitative study of three-dimensional Lagrangian particle tracking algorithms. *Exp. in Fluids*. **40**(2), 301-313 (2006).
4. *Open PTV Consortium.* Open Source Particle Tracking Velocimetry. *www.openptv.net*. (2014).
5. Parsa, S., Calzavarini, E., Toschi, F., Voth, G. Rotation Rate of Rods in Turbulent Fluid. *Phys. Rev. Lett.* **109**(13), 134501 (2012).
6. Parsa, S., Voth, G. Inertial Range Scaling in Rotations of Long Rods in Turbulence. *Phys. Rev. Lett.* **112** (2), 024501 (2014).
7. Tsai, R. A versatile camera calibration technique for high-accuracy 3d machine vision metrology using off-the-shelf tv cameras and lenses. *IEEE Journal of Robotics and Automation.* **3**(4), 323-344 (1987).
8. Blum, D., Kunwar, S., Johnson, J., Voth, G. Effects of nonuniversal large scales on conditional structure functions in turbulence. *Phys. Fluids*. **22**(1), 015107 (2010).
9. J. Mann, S. Ott, and J. S. Andersen, Experimental study of relative, turbulent diffusion, *RISO Internal Report*. **R-1036**, (1999).
10. Chan, K., Stich, D., Voth, G. Real-time image compression for high-speed particle tracking. *Rev. Sci. Instrum.*, **78**(2), 023704 (2007).
11. Goldstein, H., Poole, C., Safko, J. *Classical Mechanics, 3rd Edition.* Addison-Wesley Publishing Company, 134-180 (2002).

12. Parsa, S. Rotational dynamics of rod particles in fluid flows. *Ph.D. Thesis.* (Wesleyan University), (2013).
13. Wijesinghe, S. Measurement of the effects of large scale anisotropy on the small scales of turbulence. *Ph.D. Thesis.* (Wesleyan University), (2012).
14. Wallace, J., Foss, J. The Measurement of Vorticity in Turbulent Flows. *Annu. Rev. Fluid Mech.* **27**, 469-514 (1995).
15. Su, L., Dahm, W. Scalar imaging velocimetry measurements of the velocity gradient tensor field in turbulent flows. I. Assessment of errors. *Phys. Fluids.* **8**, 1869-1882 (1996).
16. Lüthi, B., Tsinober, A., Kinzelbach, W. Lagrangian measurement of vorticity dynamics in turbulent flow. *J. Fluid Mech.* **528**, 87-118 (2005).
17. Frish, M., Webb, W. Direct measurement of vorticity by optical probe. *J. Fluid Mech.* **107**, 173-200 (1981).
18. Zimmerman, R., *et al.* Tracking the dynamics of translation and absolute orientation of a sphere in a turbulent flow. *Rev. Sci. Instrum.* **82**(3), 033906 (2011).
19. Zimmerman, R., *et al.* Rotational Intermittency and Turbulence Induced Lift Experienced by Large Particles in a Turbulent Flow. *Phys. Rev. Lett.* **106**(15), 154501 (2011).
20. Klein, S., Gibert, Mathieu, Bérut, A., Bodenschatz, E. Simultaneous 3D measurement of the translation and rotation of finite-size particles and the flow field in a fully developed turbulent water flow. *Meas. Sci. Technol.* **24**(2), 1-10 (2013).
21. Bellani, G., Byron, M., Collignon, A., Meyer, C., Variano, E. Shape effects on turbulent modulation by large nearly neutrally buoyant particles. *J. Fluid Mech.* **712**, 41-60 (2012).

